Electrocatalysis

DOI: 10.1002/ange.201408876

Cobalt Sulfide Nanosheet/Graphene/Carbon Nanotube Nanocomposites as Flexible Electrodes for Hydrogen Evolution**

Shengjie Peng, Linlin Li, Xiaopeng Han, Wenping Sun, Madhavi Srinivasan, Subodh G. Mhaisalkar, Fangyi Cheng, Qingyu Yan,* Jun Chen, and Seeram Ramakrishna**

Abstract: *Flexible three-dimensional (3D) nanoarchitectures have received tremendous interest recently because of their potential applications in wearable electronics, roll-up displays, and other devices. The design and fabrication of a flexible and robust electrode based on cobalt sulfide/reduced graphene oxide/carbon nanotube (CoS_2/RGO-CNT) nanocomposites are reported. An efficient hydrothermal process combined with vacuum filtration was used to synthesize such composite architecture, which was then embedded in a porous CNT network. This conductive and robust film is evaluated as electrocatalyst for the hydrogen evolution reaction. The synergistic effect of CoS_2, graphene, and CNTs leads to unique CoS_2/RGO-CNT nanoarchitectures, the HER activity of which is among the highest for non-noble metal electrocatalysts, showing 10 mA cm^{-2} current density at about 142 mV overpotentials and a high electrochemical stability.*

Hydrogen is considered as one of the most ideal energy carriers that can be an alternative to fossil fuels in the future because of its numerous advantages, such as recyclability and pollution-free use.[1] Water splitting is an important method for hydrogen production in high purity and large quantities.[2] The hydrogen evolution reaction (HER) is one key step in water splitting. The use of catalysts can minimize the overpotential necessary to drive the HER in achieving a high energetic efficiency for water splitting. Although noble metals are the most active materials for the HER, their high costs greatly restrict the industrial production of hydrogen.[3] Therefore, exploring low-cost alternatives to Pt catalysts has attracted considerable attention in the past few years and still remains a major challenge. Transition-metal chalcogenides, carbides, nitrides, and metal alloys, have been widely investigated as catalysts or supports for application in the HER because of their low costs, high chemical stability, and high electrocatalytic properties.[4–6] Particularly, two-dimensional MoS_2 and WS_2 with exposed edges were demonstrated to be very promising electrocatalysts for the HER in recent years.[7–10] To stabilize the layered structure of MoS_2 during the synthesis and improve the electrical contact to the active sites, carbon materials with excellent electrical conductivity were employed as supports, such as reduced graphene oxide (RGO), carbon paper, and active carbon.[11–13] In particular, reduced graphene oxide with a high surface area can serve as host for MoS_2 and enhance the electrocatalytic HER efficiency. To improve the electrocatalytic HER efficiency, it is crucial to effectively increase the surface area for catalyst loading.[14] Furthermore, binder-free film and three-dimensional (3D) electrode structures can also effectively increase the catalyst loading and the use of catalytic sites, leading to the enhanced HER catalytic activity. As a consequence, development of advanced electrodes and optimization of the structural design is crucial to improve the catalytic performance of catalysts for the HER.

Cobalt sulfides have been previously used as electrode materials for applications in energy technologies and as catalysts for the oxygen reduction reactions (ORR),[15] however their catalytic activity towards the HER has rarely been investigated.[6,16] CoS_2, an active and low-cost electrocatalyst, can expand and enrich the family of materials suitable as efficient HER catalysts. The morphology and electrical conductivity of catalysts are the two key factors to influence the electrocatalytic efficiency. The introduction of graphene can be used as an ideal matrix for uniform growth of functional nanomaterials to improve the electrochemical activity, which would generate hybrid materials with novel properties.[17] Moreover, compared to the nanoparticle-on-sheet materials, the in situ growth of nanosheets on the RGO sheets can provide strong and stable interfacial contact with the graphene surface without aggregation and further increase electrocatalytically active sites.[18,19] Furthermore, the sheet-on-sheet structure can inhibit the aggregation of both graphene sheets and loading sheets, resulting in improved cycling performance.[18,19] Carbon nanotubes (CNTs), because of their interesting properties, nanometer size, and high surface area, have received increasing attention in recent years for their application in catalyst support materials. 3D nanostructured architectures could serve as suitable catalyst support materials, as they possess great

[*] Dr. S. Peng, Prof. S. Ramakrishna
Centre for Nanofibers and Nanotechnology
National University of Singapore
Singapore, 117576 (Singapore)
E-mail: seeram@nus.edu.sg
Dr. L. Li, W. Sun, M. Srinivasan, S. G. Mhaisalkar, Prof. Q. Yan
School of Materials Science and Engineering
Nanyang Technological, University Singapore
Singapore, 639798 (Singapore)
E-mail: alexyan@ntu.edu.sg
Dr. X. Han, Prof. F. Cheng, J. Chen
Key Laboratory of Advanced Energy Materials Chemistry (KLAEMC)
Collaborative Innovation Center of Chemical Science and Engineering, Chemistry College, Nankai University
Tianjin, 300071 (P.R. China)
E-mail: fycheng@nankai.edu.cn

[**] We gratefully acknowledge NRF (grant number CRP10-2012-06; Singapore).

Supporting information for this article is available on the WWW under http://dx.doi.org/10.1002/anie.201408876.

 © 2014 Wiley-VCH Verlag GmbH & Co. KGaA, Weinheim

potential for rapid electrochemical reactions arising from the extremely large specific surface areas for charge and mass transport.[20] Therefore, to decrease the overpotentials of electrode reactions and improve the catalytic performance, in situ growth of CoS_2 on RGO combined with CNTs is highly desirable to form a flexible 3D architecture with high electrocatalytic activity.

Herein, we report a facile wet-chemical strategy to synthesize 3D CoS_2/RGO-CNT nanocomposite architectures with high HER activity. The synthesis technique is based on a hydrothermal process to grow CoS_2 nanosheets on graphene substrates, which are then combined with CNTs by vacuum filtration. The obtained flexible and robust CoS_2/RGO-CNT film is then directly evaluated as a catalytic electrode for the HER. It is found that the highest HER activity is obtained by optimizing the amount of CNT in the composite film. Benefiting from its large specific surface area, high electrical conductivity and nanoporous structure, the CoS_2/RGO-CNT film is one of the most active non-precious metal materials for the electrochemical hydrogen evolution with low overpotential and high current densities.

The strategy for the fabrication of the CoS_2/RGO-CNT flexible film is illustrated in Scheme 1. The CoS_2 nanosheets were first in situ grown on the surface of RGO substrates

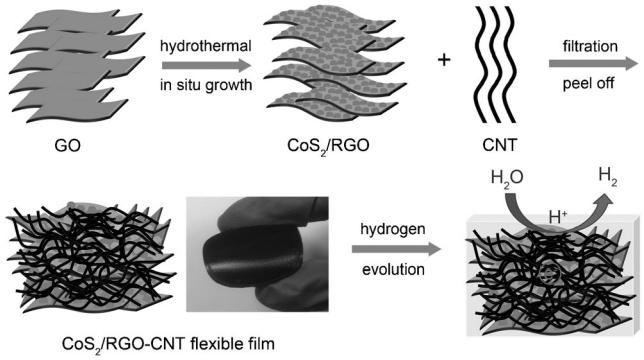

Scheme 1. Fabrication procedure and hydrogen evolution process of the freestanding CoS_2/RGO-CNT hybrid electrode.

through a simple hydrothermal process. Then the CoS_2/RGO hybrid was dispersed in a certain amount of CNT solution after sonication for several hours followed by a vacuum filtration process, which enabled the formation of 3D flexible CoS_2/RGO-CNT films. The photograph of CoS_2/RGO-CNT shows that the free-standing CoS_2/RGO-CNT film with very good flexibility can be easily bent and the high reflectivity indicates a high conductivity. By using CNTs as binder, the in situ grown CoS_2 on the RGO nanosheets was assembled into a continuous carbon skeleton and entangled into porous CNT networks, yielding a three-dimensional conductive and flexible structural CoS_2/RGO-CNT network. The resultant CoS_2/RGO-CNT film composed of a CoS_2/RGO hybrid with CNTs stacked together shows unique advantages.[20]

In our method, RGO has been considered as an ideal substrate for ultrathin coating of functional materials because of its unique structural and electrical properties, while the uniformly interconnected CNT network with the highly conductive and porous properties is beneficial for electronic and ionic transport. The CoS_2 nanosheets grown on the RGO can enhance the effective interaction between the active materials and the electrolyte, compared to the physical mixing of catalyst and carbon materials, which could not fully capture the properties of the catalyst and carbon due to aggregation, phase separation, and poor connectivity between catalysts and carbon. Furthermore, the procedure is very simple by using CoS_2/RGO and CNT as raw materials without any polymer binder in the film, which enables excellent electrical and mechanical properties. With CoS_2/RGO uniformly distributed in the highly conductive CNT network, the 3D hierarchical structure can provide a robust electrical connection within the entire electrode framework, enable the contact with the liquid electrolyte readily, and even maintain such features during the cycling process because of the 3D wrapping effect of the CNTs.[20] Such continuous 3D network finally can render well-developed porous structures, high mechanical strength, and superior flexibility of the composites. Therefore, the CoS_2/RGO-CNT composite is considered as an ideal HER catalyst.

The morphology and purity of the CoS_2/RGO composite was characterized using scanning electron microscopy (SEM), transmission electron microscopy (TEM), high-magnified transmission electron microscopy (HRTEM), and X-ray diffraction (XRD). As shown in Figure 1 a–c, the RGO sheets with a size of about several micrometers are uniformly decorated with CoS_2 ultrathin nanosheets. The cross-sectional SEM image of a part of the CoS_2/RGO composites in Figure 1 c shows that CoS_2 nanosheets grow on both sides of the RGO sheets, and several layers of such composites arrange in an orderly fashion to form an interesting hierarchical architecture. The formation of the unique CoS_2/RGO structure went through nucleation and growth processes on the RGO matrix as shown by time-dependent experiments (Figure S1 in the Supporting Information). When GO was absent, the material tended to form hollow spherical structures (Figure S2). A more revealing feature of the CoS_2-RGO sheet-on-sheet structure can be seen from Figure 1 d–f. The TEM image in Figure 1 d shows that most of the CoS_2 nanosheets lie vertically on graphene. A vertical CoS_2 nanosheet indicates the thickness of about 4 nm (Figure 1 e). The lattice spacing is measured to be about 0.277 and 0.323 nm, which can be assigned to the (200) and (111) planes of the cubic CoS_2 phase, respectively (Figure 1 f). The phase of the CoS_2-RGO hybrid is characterized by X-ray diffraction (XRD), which is shown in Figure 1 g. It is observed that all the diffraction peaks are attributed to the cubic CoS_2 phase (JCPDS number 41-1471). No diffraction peaks for RGO can be observed in the pattern because of its low amount and relatively low diffraction intensity. Furthermore, the purity of CoS_2 was demonstrated by X-ray photoelectron spectroscopy (XPS) (Figure S3).[21] The high-frequency infrared carbon–sulfur analyzer shows that the composite consists of 10.2 wt % carbon. The presence of RGO can be confirmed by analysis of the Raman spectrum. Two characteristic peaks of the D and G bands of the CoS_2-RGO hybrid are observed at about 1340 and 1590 cm^{-1} (Figure 1 h), respectively. The intensity ratios of the D to G bands were 0.91 and 1.08 for GO and the CoS_2-

 © 2014 Wiley-VCH Verlag GmbH & Co. KGaA, Weinheim

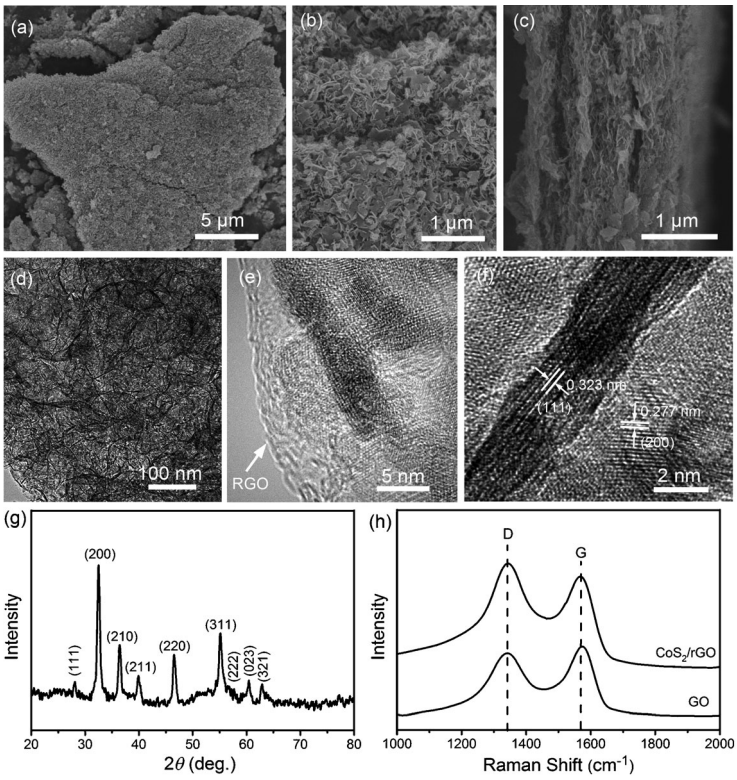

Figure 1. a–c) SEM images, d–f) TEM images, g) XRD pattern and h) Raman spectrum of the CoS_2/RGO hybrid.

RGO hybrid, respectively. The higher ratio for CoS_2-RGO relative to GO indicates that GO was reduced to some extent, which is consistent with a previous report.[12] The hierarchical CoS_2/RGO composite has a high surface area of 193.5 $mg\,cm^{-2}$ (Figure S4). This demonstrates that thin CoS_2 nanosheets deposited on graphene sheets can be obtained under the present hydrothermal process.

The CoS_2/RGO-CNT hybrid electrode was obtained from a simple vacuum filtration of a mixture containing the CoS_2/RGO hybrid and CNTs (diameter of 10–20 nm and length of several tens of micrometers; Figure S5). At least 30 mg CNTs in the filter precursor solution were required to enable the composite to form a flexible film. And the higher amount of CNTs could lead to a film with higher flexibility and higher mechanically strength. Figure 2a,b shows the top view and cross-sectional SEM images of the CoS_2/RGO-CNT film. The CoS_2/RGO composites were tightly trapped and uniformly distributed in the porous CNT network. The intimate contacts between the composite particles and CNTs provide robust electrical conductive pathways, which are critical for catalytic applications. The TEM image in Figure 2c reveals that CoS_2/RGO maintains its sheet-on-sheet structure and is mixed well with CNTs. After filtration, the hybrid can form a flexible film with a thickness of about 100 μm (inset of Figure 2a). Moreover, the resulting 3D hierarchical film shows high flexibility and good mechanical strength. Figure 2d shows a typical stress–strain curve of the 3D film, which displays an average tensile strength of 32 MPa at a strain of 2.0%. Accordingly, the Young's modulus of the film is about 1.3 GPa. The mechanical reinforcement originates from the entanglement of the CNT network. Such strong composite electrodes ensure structure stability and are rarely achieved. Furthermore, the binder-free CoS_2/RGO-CNT composite possess a much higher electrical conductivity ($7.2\times10^{-2}\ S\,m^{-1}$) than a conventional electrode ($2.5\times10^{-3}\ S\,m^{-1}$) using Nafion as the binder. Both the high strength and conductivity of the binder-free CoS_2/RGO-CNT composite are beneficial for achieving better catalytic stability and smaller electrode polarization.

The free-standing CoS_2/RGO-CNT film was directly investigated as an electrocatalyst for the HER. The CoS_2 loading in the film is about

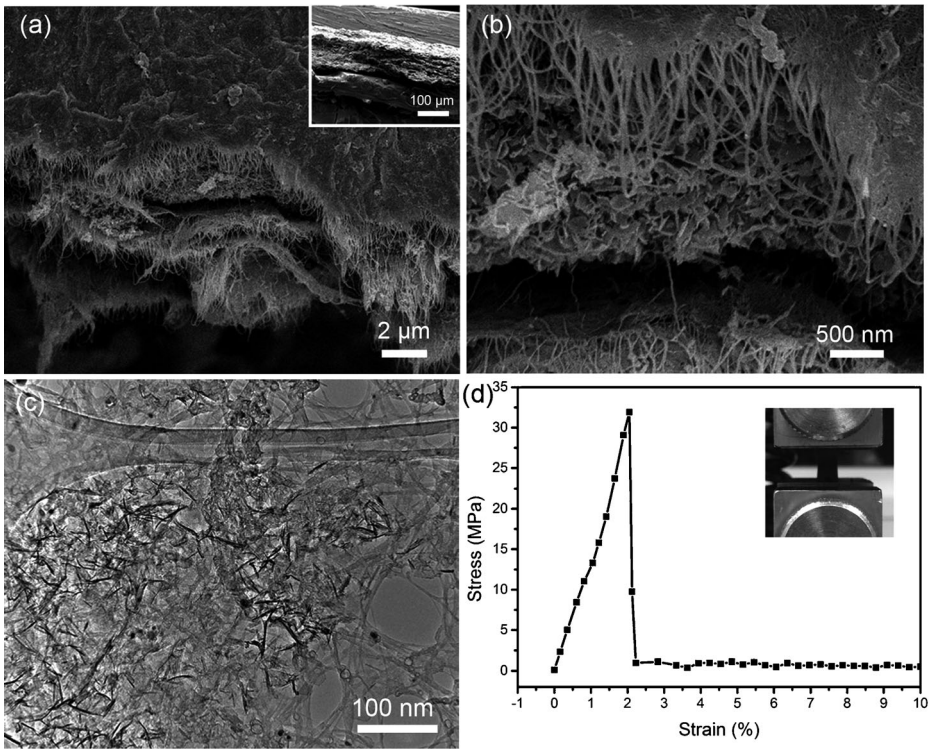

Figure 2. a) Cross-sectional and b) corresponding magnified SEM, and c) TEM images of the interconnected structure formed by the CoS_2/RGO composite and CNTs. The inset indicates the thickness of the composite film. d) Typical stress–strain curve for the CoS_2/RGO-CNT composite film.

© 2014 Wiley-VCH Verlag GmbH & Co. KGaA, Weinheim

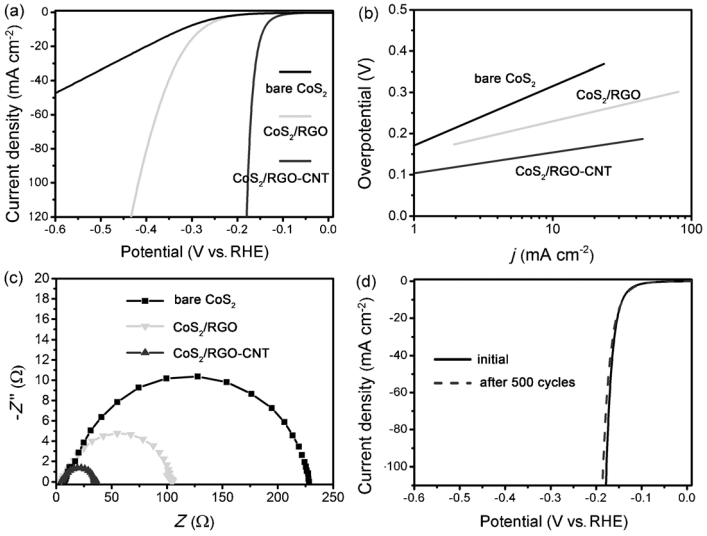

Figure 3. a) Polarization curves, b) Tafel plots, and c) Nyquist plots of the bare CoS_2 and CoS_2/RGO on glassy carbon substrates, and free-standing CoS_2/RGO-CNT film electrodes in 0.5 M H_2SO_4, respectively. d) Stability test for the CoS_2/RGO-CNT electrode.

1.15 mg cm^{-2}. Bare CoS_2 and the CoS_2/RGO sample were also tested as a reference. Figure 3a shows the polarization curves of the samples measured in a 0.5 M H_2SO_4 solution with a scan rate of 2 mV s^{-1} at room temperature. The polarization curve recorded by the as-prepared CoS_2/RGO-CNT showed a low overpotential of 142, 153, and 178 mV at current densities (j) of 10, 20, and 100 mA cm^{-2}, respectively. In contrast, bare CoS_2 or CoS_2/RGO powder exhibited overpotentials of 398 and 313 mV at a current density of 20 mA cm^{-2}, which is much lower than the overpotential observed for CoS_2/RGO-CNT, indicating their inferior HER catalytic activity. Also, the CNT has little HER activity in acidic solution (Figure S6 in the Supporting Information). To further evaluate the intrinsic activity of the new composite catalyst, the exchange current density (j_0) is determined by fitting polarization data to the Tafel equation ($\eta = b \log j + a$, where j is the current density and b is the Tafel slope).[8b] The j_0 for the CoS_2/RGO-CNT film was determined as 6.26×10^{-5} A cm^{-2}, outperforming the value of 1.01×10^{-6} and 7.02×10^{-6} A cm^{-2} of bare CoS_2 and CoS_2/RGO. It can be summarized that the overpotentials and exchange current density of CoS_2/RGO-CNT compare favorably and even superior to the behavior of other non-Pt HER electrocatalysts in acidic aqueous solutions, including the CoP/Ti foil,[4a] CoS_2/graphite,[6c] and $CoSe_2$/carbon paper.[12c] Although the HER activity of commercial Pt/C is higher than that of CoS_2/RGO-CNT, CoS_2/RGO-CNT is one of the best Pt-free HER catalysts with similar mass loadings, in terms of exchange current densities and exchange current densities normalized by surface area and catalyst mass (Figures S7–S11 and Tables S1–S3). Furthermore, the different loading measurements suggest that 1.15 mg cm^{-2} is the optimal loading in our system (Figure S9).

The polarization curves showed that the catalytic current density of CoS_2/RGO-CNT was the highest of all samples, indicating that both the conductive CNT skeleton and unique structure of the in situ grown CoS_2 on RGO were important to enhance the electrocatalytical activity of CoS_2/RGO-CNT for the HER. The higher electrocatalytic activity of CoS_2/RGO-CNT may be attributable to its more active sites, originating from its unique structural characteristics. The separated nanosheets with loosely stacked layers provide highly exposed rims and edges, which afford abundant accessible catalytic sites for H^+ adsorption and the HER.[22] Furthermore, the free-standing CoS_2/RGO-CNT film shows a higher polarization current density than CoS_2 grown on other substrates such as graphite paper, Ti foil, and carbon cloth, which indicates superiority of the unique 3D network structure (Figures S12 and S13).

The Tafel plots derived from Figure 3a are shown in Figure 3b, where their linear portions were fitted to the Tafel equation to determine Tafel slopes. A smaller Tafel slope of about 51 mV decade^{-1} was observed for the CoS_2/RGO-CNT catalyst, which is much smaller than the slope observed for the CoS_2/RGO powder (82 mV decade^{-1}) and bare CoS_2 (148 mV decade^{-1}). The value suggests that the Volmer–Heyrovsky mechanism takes effect in the HER of CoS_2/RGO-CNT.[5] In principle, a lower Tafel slope means that a catalyst requires a lower applied overpotential to generate a required current.[22] Therefore, the CoS_2/RGO-CNT with the smallest slope value displays the best activity in the HER. The Tafel slope value of the CoS_2/RGO-CNT catalyst compares favorably to those observed for other non-noble-metal catalysts, such as MoS_2/carbon fiber paper (62 mV decade^{-1}),[23a] CoP/carbon cloth (51 mV decade^{-1}),[23b] $W(S_{0.48}Se_{0.52})_2$ (105 mV decade^{-1}),[23c] and CoS_2/graphite (51.6 mV decade^{-1}).[6c]

To further investigate the effect of the free-standing film on the HER activity, we preformed electrochemical impedance spectroscopy (EIS) analysis of CoS_2, CoS_2/RGO, and CoS_2/RGO-CNT. The obtained Nyquist plot is shown in Figure 3c. The semicircle in the high-frequency range of the Nyquist plot attributed to the charge-transfer resistance R_{ct} is related to the electrocatalytic kinetics and a lower value corresponds to a faster reaction rate.[24] The R_{ct} value of the bare CoS_2 electrode is the smallest among all the composite catalysts; therefore, CoS_2/RGO-CNT shows the best HER activity, which is consistent with the result obtained from polarization measurements (Figure 3a). The low charge-transfer resistance is beneficial to achieve highly efficient charge transport, owing to the synergistic effect from the CoS_2 growth on RGO sheets and the excellent electrical coupling to the conductive MWCNT network.

High durability is another important concern for a good electrocatalyst. For the assessment of this parameter, the CoS_2/RGO-CNT catalyst electrode was cycled continuously for 500 cycles. Figure 3d shows the polarization plots after the first cycle and at the end of cycling. No obvious decay of the activity was observed, suggesting high catalytic durability of the novel CoS_2/RGO-CNT electrocatalyst below 0 V in acidic electrolyte. It should be noted that the cyclic voltammetry measurement indicates that the film could be oxidized at about 0.37 V versus reversible hydrogen electrode (RHE; Figure S14). The considerable catalytic durability is probably

 © 2014 Wiley-VCH Verlag GmbH & Co. KGaA, Weinheim

attributed to the tight binding between the active material and the substrate by the in situ fabrication approach and robust feature of the 3D film.

In summary, we have developed a facile method to produce a highly active, stable 3D CoS_2/G-CNT nanoarchitecture by combining hydrothermal treatment and vacuum filtration. The obtained flexible and robust film can be directly used as the catalytic electrode for the HER. The synergistic effect from CoS_2, graphene, and CNTs may contribute to the high HER activity of this material. Furthermore, the unique 3D nanoporous structure leads to high catalytic stability in the long-term operation. To the best our knowledge, this new 3D CoS_2/G-CNT nanoarchitecture film is one of the best non-precious electrocatalysts for the HER in acidic medium. This work presents a new strategy for designing advanced non-noble metal catalysts and helps to enable the widespread deployment of cost-effective systems for the electrochemical hydrogen production. Significantly, this effective strategy might be extended to construct many other composite electrodes for high-performance HER catalysis, batteries, and supercapacitors.

Received: September 7, 2014
Published online: October 8, 2014

Keywords: cobalt sulfide · flexible electrodes · graphene · hybrid composites · hydrogen evolution reaction

[1] a) J. Greeley, T. F. Jaramillo, J. Bonde, I. Chorkendorff, J. K. Nørskov, *Nat. Mater.* **2006**, *5*, 909 – 913; b) M. G. Walter, E. L. Warren, J. R. McKone, S. W. Boettcher, Q. X. Mi, E. A. Santori, N. S. Lewis, *Chem. Rev.* **2010**, *110*, 6446 – 6473.

[2] a) J. Kibsgaard, Z. B. Chen, B. N. Reinecke, T. F. Jaramillo, *Nat. Mater.* **2012**, *11*, 963 – 969; b) S. B. Yang, Y. J. Gong, J. S. Zhang, L. Zhan, L. L. Ma, Z. Y. Fang, R. Vajtai, X. C. Wang, P. M. Ajayan, *Adv. Mater.* **2013**, *25*, 2452 – 2456; c) H. M. Chen, C. K. Chen, R. S. Liu, L. Zhang, J. J. Zhang, D. P. Wilkinson, *Chem. Soc. Rev.* **2012**, *41*, 5654 – 5671.

[3] a) B. Fang, J. Kim, J. S. Yu, *Electrochem. Commun.* **2008**, *10*, 659 – 662; b) Z. Varpness, J. W. Peters, M. Young, T. Douglas, *Nano Lett.* **2005**, *5*, 2306 – 2309; c) S. A. Grigoriev, P. Millet, V. N. Fateev, *J. Power Sources* **2008**, *177*, 281 – 285.

[4] a) E. J. Popczun, C. G. Read, C. W. Roske, N. S. Lewis, R. E. Schaak, *Angew. Chem. Int. Ed.* **2014**, *53*, 5427 – 5430; *Angew. Chem.* **2014**, *126*, 5531 – 5534; b) Y. F. Xu, M. R. Gao, Y. R. Zheng, J. Jiang, S. H. Yu, *Angew. Chem. Int. Ed.* **2013**, *52*, 8546 – 8550; *Angew. Chem.* **2013**, *125*, 8708 – 8712; c) Y. D. Hou, A. B. Laursen, J. H. Zhang, G. G. Zhang, Y. S. Zhu, X. C. Wang, S. Dahl, I. Chorkendorff, *Angew. Chem. Int. Ed.* **2013**, *52*, 3621 – 3625; *Angew. Chem.* **2013**, *125*, 3709 – 3713; d) Q. Liu, J. Q. Tian, W. Cui, P. Jiang, N. Y. Cheng, A. M. Asiri, X. P. Sun, *Angew. Chem. Int. Ed.* **2014**, *53*, 6710 – 6714; *Angew. Chem.* **2014**, *126*, 6828 – 6832.

[5] a) Y. Zheng, Y. Jiao, Y. H. Zhu, L. H. Li, Y. Han, Y. Chen, A. J. Du, M. Jaroniec, S. Z. Qiao, *Nat. Commun.* **2014**, *5*, 3783; b) W. F. Chen, J. T. Muckerman, E. Fujita, *Chem. Commun.* **2013**, *49*, 8896 – 8909; c) W. F. Chen, K. Sasaki, C. Ma, A. I. Frenkel, N. Marinkovic, J. T. Muckerman, Y. M. Zhu, R. R. Adzic, *Angew. Chem. Int. Ed.* **2012**, *51*, 6131 – 6135; *Angew. Chem.* **2012**, *124*, 6235 – 6239.

[6] a) D. S. Kong, J. J. Cha, H. T. Wang, H. R. Lee, Y. Cui, *Energy Environ. Sci.* **2013**, *6*, 3553 – 3559; b) P. D. Tran, S. Yang Chiam, P. P. Boix, Y. Ren, S. S. Pramana, J. Fize, V. Artero, J. Barber, *Energy Environ. Sci.* **2013**, *6*, 2452 – 2459; c) M. S. Faber, R. Dziedzic, M. A. Lukowski, N. S. Kaiser, Q. Ding, S. Jin, *J. Am. Chem. Soc.* **2014**, *136*, 10053 – 10061.

[7] a) J. F. Xie, H. Zhang, S. Li, R. X. Wang, X. Sun, M. Zhou, J. F. Zhou, X. W. Lou, Y. Xie, *Adv. Mater.* **2013**, *25*, 5807 – 5813; b) J. Yang, D. Voiry, S. J. Ahn, D. Kang, A. Y. Kim, M. Chhowalla, H. S. Shin, *Angew. Chem. Int. Ed.* **2013**, *52*, 13751 – 13754; *Angew. Chem.* **2013**, *125*, 13996 – 13999.

[8] a) M. A. Lukowski, A. S. Daniel, F. Meng, A. Forticaux, L. S. Li, S. Jin, *J. Am. Chem. Soc.* **2013**, *135*, 10274 – 10277; b) A. B. Laursen, S. Kegnæs, S. Dahl, I. Chorkendorff, *Energy Environ. Sci.* **2012**, *5*, 5577 – 5591.

[9] a) D. S. Kong, H. T. Wang, J. J. Cha, M. Pasta, K. J. Koski, J. Yao, Y. Cui, *Nano Lett.* **2013**, *13*, 1341 – 1347; b) D. Voiry, M. Salehi, R. Silva, T. Fujita, M. W. Chen, T. Asefa, V. B. Shenoy, G. Eda, M. Chhowalla, *Nano Lett.* **2013**, *13*, 6222 – 6227.

[10] U. Maitra, U. Gupta, M. De, R. Datta, A. Govindaraj, C. N. R. Rao, *Angew. Chem. Int. Ed.* **2013**, *52*, 13057 – 13061; *Angew. Chem.* **2013**, *125*, 13295 – 13299.

[11] a) X. L. Huang, R. Z. Wang, D. Xu, Z. L. Wang, H. G. Wang, J. J. Xu, Z. Wu, Q. C. Liu, Y. Zhang, X. B. Zhang, *Adv. Funct. Mater.* **2013**, *23*, 4345 – 4353; b) L. Liao, J. Zhu, X. J. Bian, L. Zhu, M. D. Scanlon, H. H. Girault, B. H. Liu, *Adv. Funct. Mater.* **2013**, *23*, 5326 – 5333; c) Y. J. Gong, S. B. Yang, Z. Liu, L. L. Ma, R. Vajtai, P. M. Ajayan, *Adv. Mater.* **2013**, *25*, 3979 – 3984.

[12] a) Y. G. Li, H. L. Wang, L. M. Xie, Y. Y. Liang, G. S. Hong, H. J. Dai, *J. Am. Chem. Soc.* **2011**, *133*, 7296 – 7299; b) X. J. Bian, M. D. Scanlon, S. Wang, L. Liao, Y. Tang, B. H. Liu, H. H. Girault, *Chem. Sci.* **2013**, *4*, 3432 – 3441; c) D. S. Kong, H. T. Wang, Z. Y. Lu, Y. Cui, *J. Am. Chem. Soc.* **2014**, *136*, 4897 – 4900.

[13] E. G. S. Firmiano, M. A. L. Cordeiro, A. C. Rabelo, C. J. Dalmaschio, A. N. Pinheiro, E. C. Pereira, E. R. Leite, *Chem. Commun.* **2012**, *48*, 7687 – 7689.

[14] a) Y. Huang Chang, F. Y. Wu, T. Y. Chen, C. L. Hsu, C. H. Chen, F. Wiryo, K. H. Wei, C. Y. Chiang, L. J. Li, *Small* **2014**, *10*, 895 – 900; b) Y. H. Chang, C. T. Lin, T. Y. Chen, C. L. Hsu, Y. H. Lee, W. J. Zhang, K. H. Wei, L. J. Li, *Adv. Mater.* **2013**, *25*, 756 – 760.

[15] a) S. J. Peng, L. L. Li, H. T. Tan, R. Cai, W. H. Shi, C. C. Li, S. G. Mhaisalkar, M. Srinivasan, S. Ramakrishna, Q. Y. Yan, *Adv. Funct. Mater.* **2014**, *24*, 2155 – 2162; b) H. L. Wang, Y. Y. Liang, Y. G. Li, H. J. Dai, *Angew. Chem. Int. Ed.* **2011**, *50*, 7364 – 7368; *Angew. Chem.* **2011**, *123*, 7502 – 7506; c) Y. J. Feng, T. He, N. Alonso-Vante, *Chem. Mater.* **2008**, *20*, 26 – 28; d) Q. H. Wang, L. F. Jiao, Y. Han, H. M. Du, W. X. Peng, Q. N. Huan, D. W. Song, Y. C. Si, Y. J. Wang, H. T. Yuan, *J. Phys. Chem. C* **2011**, *115*, 8300 – 8304.

[16] L. Cheng, W. J. Huang, Q. F. Gong, C. H. Liu, Z. Liu, Y. G. Li, *Angew. Chem. Int. Ed.* **2014**, *53*, 7860 – 7863; *Angew. Chem.* **2014**, *126*, 7994 – 7997.

[17] a) Z. S. Wu, D. W. Wang, W. C. Ren, J. P. Zhao, G. M. Zhou, F. Li, H. M. Cheng, *Adv. Funct. Mater.* **2010**, *20*, 3595 – 3602; b) G. Q. Zhang, B. Y. Xia, X. Wang, X. W. Lou, *Adv. Mater.* **2014**, *26*, 2408 – 2412.

[18] J. X. Zhu, Y. K. Sharma, Z. Y. Zeng, X. J. Zhang, M. Srinivasan, S. Mhaisalkar, H. Zhang, H. H. Hng, Q. Y. Yan, *J. Phys. Chem. C* **2011**, *115*, 8400 – 8406.

[19] Y. Liu, D. Yan, R. F. Zhuo, S. K. Li, Z. G. Wu, J. Wang, P. Y. Ren, P. X. Yan, Z. R. Geng, *J. Power Sources* **2013**, *242*, 78 – 85.

[20] a) S. Luo, K. Wang, J. P. Wang, K. L. Jiang, Q. Q. Li, S. S. Fan, *Adv. Mater.* **2012**, *24*, 2294 – 2298; b) Y. W. Cheng, S. T. Lu, H. B. Zhang, C. V. Varanasi, J. Liu, *Nano Lett.* **2012**, *12*, 4206 – 4211; c) X. L. Jia, Z. Chen, X. Cui, Y. T. Peng, X. L. Wang, G. Wang, F. Wei, Y. F. Lu, *ACS Nano* **2012**, *6*, 9911 – 9919.

[21] a) L. Zhu, D. Susac, M. Teo, K. C. Wong, P. C. Wong, R. R. Parsons, D. Bizzotto, K. A. R. Mitchell, S. A. Campbell, *J. Catal.* **2008**, *258*, 235 – 242; b) S. J. Peng, L. L. Li, S. G. Mhaisalkar, M.

 © 2014 Wiley-VCH Verlag GmbH & Co. KGaA, Weinheim

Srinivasan, S. Ramakrishna, Q. Y. Yan, *ChemSusChem* **2014**, *7*, 2212 – 2220.
[22] D. Merki, X. L. Hu, *Energy Environ. Sci.* **2011**, *4*, 3878 – 3888.
[23] a) H. T. Wang, Z. Y. Lu, D. S. Kong, J. Sun, T. M. Hymel, Y. Cui, *ACS Nano* **2014**, *8*, 4940 – 4947; b) J. Q. Tian, Q. Liu, A. M. Asiri, X. P. Sun, *J. Am. Chem. Soc.* **2014**, *136*, 7587 – 7590; c) K. Xu, F. M. Wang, Z. X. Wang, X. Y. Zhan, Q. S. Wang, Z. Z. Cheng, M. Safdar, J. He, *ACS Nano* **2014**, *8*, 8468 – 8476.
[24] a) Y. Yan, X. M. Ge, Z. L. Liu, J. Y. Wang, J. M. Lee, X. Wang, *Nanoscale* **2013**, *5*, 7768 – 7771; b) D. Merki, H. Vrubel, L. Rovelli, S. Fierro, X. L. Hu, *Chem. Sci.* **2012**, *3*, 2515 – 2525.

 © 2014 Wiley-VCH Verlag GmbH & Co. KGaA, Weinheim